Unusual Catalytic Properties of High Energetic Facet Polar Metal Oxides

*Yiyang Li and Shik Chi Edman Tsang**

Wolfson Catalysis Centre, Department of Chemistry, University of Oxford, OX1 3QR, UK

Conspectus: Heterogeneous catalysis is an area of great importance not only in chemical industries, but also in energy conversion and environmental technologies. It is well established that specific surface morphology and structure of solid catalysts exert remarkable effects on catalytic performances, since most physical and chemical processes take place on the surface during catalytic reactions. Different from the widely studied faceted metallic nanoparticles, metal oxides give more complicated structures and surface features. Great progress has been achieved in controlling the shape and exposed facets of transition metal oxides during the nanocrystal growth, usually by using surface directing agents (SDAs). However, the effects of exposed facets remain controversial among researchers. It should be noted that the high-energy facets, especially the polar facets tend to lower their surface energy via different relaxation processes, such as surface reconstruction, redox change or adsorption of counter-charged species, etc. These processes can subsequently lead to surface defect formation and break the surface stoichiometry, and the resulted changes of electronic configurations and charge migration properties all play important roles in heterogeneous catalysis. Given that different materials prefer different relaxation methods, thus various surface features are created and different techniques are required to investigate the different features from facet to facet. Conventional characterization techniques such as X-ray diffraction (XRD), X-ray photoelectron spectroscopy (XPS), transmission electron microscopy

(TEM), etc. appear to be insufficient to elucidate the underlying principles of the facet effects. Consequently, increasing number of novel techniques have been developed to differentiate the surface features, enabling more understandings of the facet effects on heterogeneous catalysis.

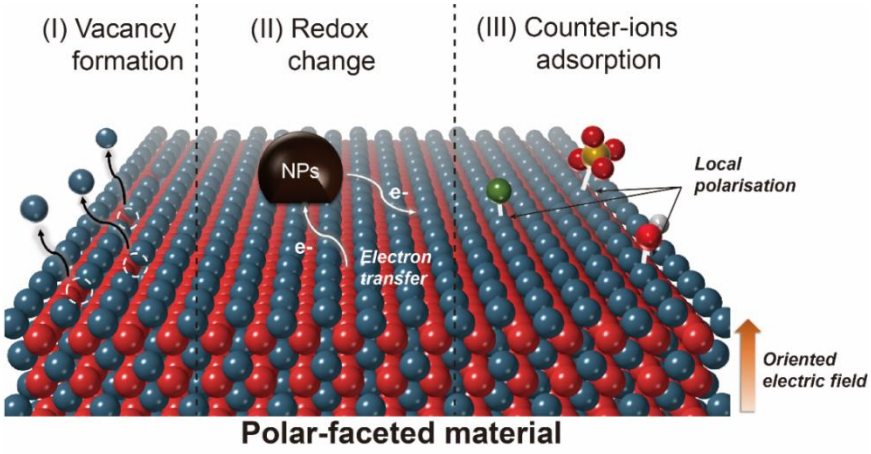

Herein, based on the previous studies of our own group, we will focus on the effects of tailored facet on heterogeneous catalysis introduced by engineered simple binary metal oxide nanomaterials primarily with exposed polar facets, in combination with detailed surface study by a range of new characterization techniques. As a result, fundamental principles of the facet effects are elucidated and the structure-activity correlations are demonstrated. The surface features introduced by different relaxation processes are also investigated by a range of characterization techniques. For example, electron paramagnetic resonance (EPR) is used to detect the oxygen vacancies, while probe-assisted solid-state nuclear magnetic resonance (ssNMR) is shown to be facet-sensitive and able to evaluate the surface acidity. It is also shown that such different features influence the heterogeneous catalytic performances in different ways. With the help of first-principles density functional theory (DFT) calculations, unique properties of the faceted metal oxides are discussed and unraveled. Besides, other materials like transition metal chalcogenides

and layered double hydroxides (LDHs) will also be briefly discussed about their application in the facet-dependent catalysis studies.

Key References:

1. Wu, S.; Peng, Y.-K.; Large, A. I.; Zheng, J.; Chen, T.; Duan, H.; McPherson, I. J.; Wilkinson, I.; Chou, H.-L.; Held, G.; Chi, S.; Tsang, S. C. E. Removal of Hydrogen Poisoning by Polar MgO Support for Low Pressure NH3 Synthesis at Unprecedented Rate over Ru Catalyst. *ACS Catal.* **2020,** *10*, 5614–5622.[1] *Polar-faceted MgO(111) decorated with Ru was proved to show a stable and record-high ammonia synthesis activity due to the local electric field, giving an activity of 4.5 times as high as the commercial MgO catalyst.*

2. Ye, L.; Duan, X.; Wu, S.; Wu, T. S.; Zhao, Y.; Robertson, A. W.; Chou, H. L.; Zheng, J.; Ayvalı, T.; Day, S.; Tang, C.; Soo, Y. L.; Yuan, Y.; Tsang, S. C. E. Self- Regeneration of Au/CeO_2 Based Catalysts with Enhanced Activity and Ultra-Stability for Acetylene Hydrochlorination. *Nat. Commun.* **2019**, *10*, 914.[2] *Au/activated carbon catalyst showed self-regeneration ability after the inclusion of facet-engineered CeO_2 nanorods, resulting in superior performances in the acetylene hydrochlorination reaction with stable activity for more than 3000 h.*

3. Li, Y.; Peng, Y.-K.; Hu, L.; Zheng, J.; Prabhakaran, D.; Wu, S.; Puchtler, T. J.; Li, M.; Wong, K.-Y.; Taylor, R. A.; Tsang, S. C. E. Photocatalytic water splitting by N-TiO_2 on MgO (111) with exceptional quantum efficiencies at elevated temperatures. *Nat. Commun.* **2019**, *10*, 4421.[3] *Photocatalytic performances of N-doped TiO_2 was improved after combined with polar-faceted metal oxides, giving extraordinary activities and quantum efficiencies in the photocatalytic overall water splitting reaction. Such enhancement was due to the local electric field of the polar surfaces.*

4. Peng, Y. K.; Ye, L.; Qu, J.; Zhang, L.; Fu, Y.; Teixeira, I. F.; McPherson, I. J.; He, H.; Tsang, S. C. E. Trimethylphosphine-Assisted Surface Fingerprinting of Metal Oxide Nanoparticle by

^{31}P Solid-State NMR: A Zinc Oxide Case Study. *J. Am. Chem. Soc.* **2016**, *138* (7), 2225–2234.[4]
Solid-state ^{31}P NMR was used to map various ZnO surfaces with trimethylphosphine as probe. And it was demonstrated that this technique could provide qualitative and quantitative information of the surface features on different facets from a single deconvoluted spectrum.

1. Introduction

Nanomaterials are ubiquitously engaged as heterogeneous catalysts due to exceptional physicochemical properties. The surface of these catalyst particles provides the platform for catalytic reactions.[5] Since the environment of surface atoms is quite different from that of the bulk, one would expect distinct properties on crystal surfaces.[6] Up to now, most facet engineering studies are on metallic nanoparticles (NPs), which are commonly active components in heterogeneous catalysts.[7–11] Our group studied the catalytic performances of metallic NPs and investigated the effect of size, shape, surface features, local factors, etc. Different PVP-stabilized metallic NPs were investigated by ^{13}C NMR under catalytic conditions in the liquid phase in an early work, where the catalytic performances on decomposition of formic acid were tested.[12] Our recent work illustrated that the Ag nanocubes with dominantly exposed (100) facets exhibited superior HER activity over Pt in the PEM electrolyzer when practically more negative potential was applied.[13] Various bimetallic core-shell nanoparticles have been rationally designed and fabricated as well, showing promising activities toward formic acid electrooxidation.[12,14]

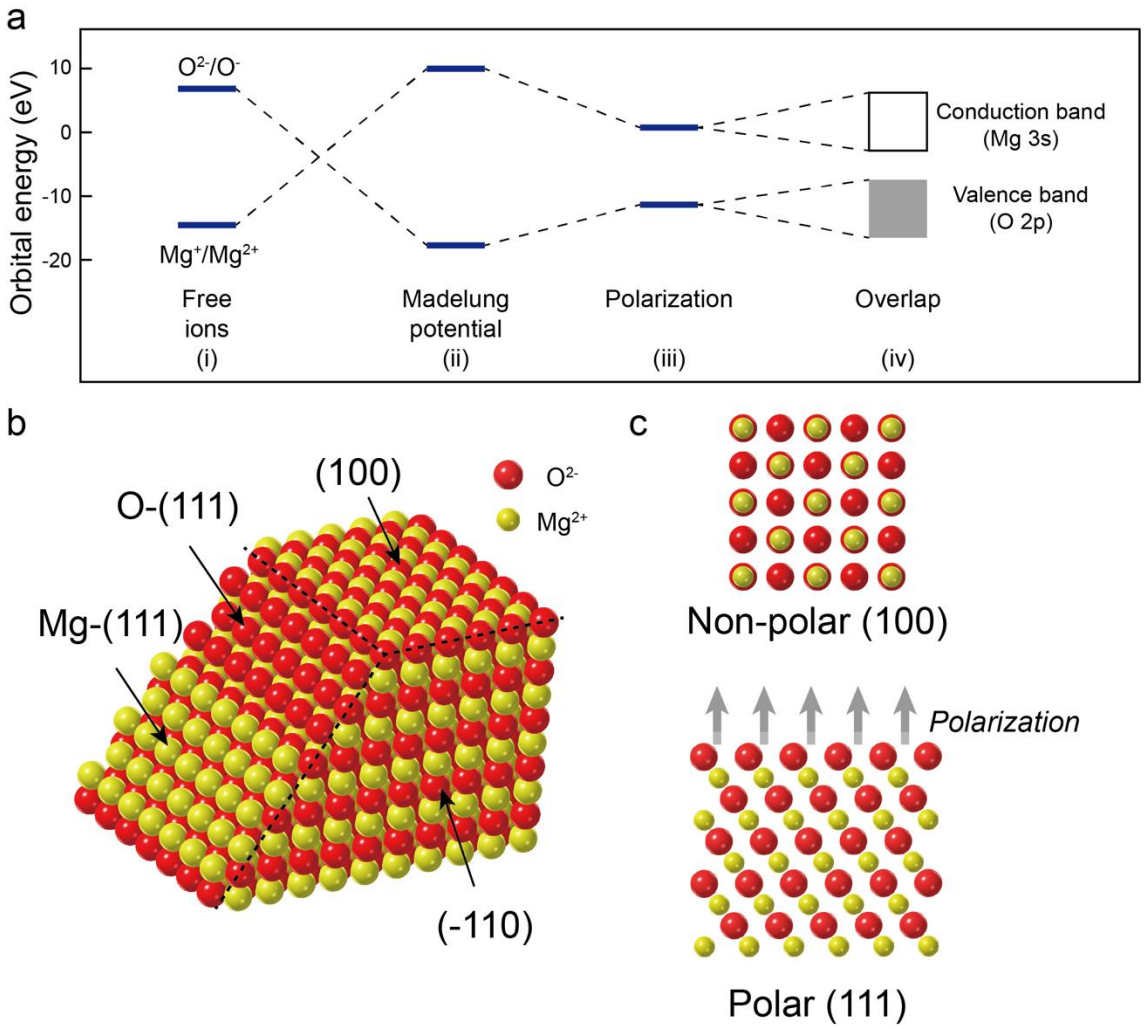

Fig. 1 Ionic model of MgO: (a) the orbital energies of filled oxygen 2p and empty magnesium 3s levels under different states; (b) Structural model of different exposed facets; (c) Crystal packing of polar and non-polar faceted MgO. Arrows indicated the polarization near the polar surface.

Given that the facet engineering of metallic NPs has been comprehensively studied and reviewed, facet-dependent catalysis of metal oxide nanocrystals that finds wide applications in chemical industries, energy conversion and environmental technologies is not yet clear. Unlike metallic NPs, binary metal oxides are more complicated, and the underpinning principles of their catalytic effects remain controversial. Taking a simple ionic model of MgO as an example, Fig. 1a shows the

energy levels of filled oxygen 2p and unfilled magnesium 3s orbitals. For these isolated hard ionic species, the ionic charge distribution Mg^{2+}-O^{2-} is clearly not stable in the gas phase and the O^{2-} ion does not even exist since the second electron affinity of O^- is highly endothermic. However, these ions can be stabilized in a solid ionic lattice, so they experience a summation of long-range Coulomb potentials from the ions in the lattice positions so called *Madelung potential* of appropriate sign. At oxide sites, the *Madelung potential* is positive, thus stabilizes electrons; at cation sites it is negative and correspondingly destabilizing as shown in the figure. Thus, the most stable crystal structure is composed of ions interspersed with nearby counter-ions and so on in the lattice. If some charges dislocate from the lattice, polarization occurs. The effect of polarization has been shown by lowering the energy of empty (metal) levels and raising that of filled (oxygen) levels; hence the binding energies for electrons in filled levels will be reduced. Finally, the broadening of electronic levels gives bands, rather than discrete energy levels, due to overlapping between ions.

In the crystal facets, similar ion distributions exist in the energy minimized packing (Figs. 1b and 1c). The most stable surfaces of MgO in this case, are (100) or (-110) where cations and anions are evenly inter-dispersive, obtaining the Madelung stabilization. Although exposure of high-energy facets such as O- or Mg-terminated (111) is thermodynamically unfavorable, it can be kinetically controlled during the crystal growths. It is noteworthy that these thermodynamically unstable high-energy facets tend to reduce the surface energy through relaxation process,[15] which can exert unusual effects such as band gap reduction, excitons stabilization, enhanced adsorption of counter-ions and induced surface reconstruction. However, it is highly material dependent (for example, reduction of hard ions, like Mg^{2+} to Mg^+ is energetically not favorable due to

destabilizing lattice energy but is not the case for Ce^{4+} to Ce^{3+}). More details about the nature of polar surface can be found in the Supporting Information.

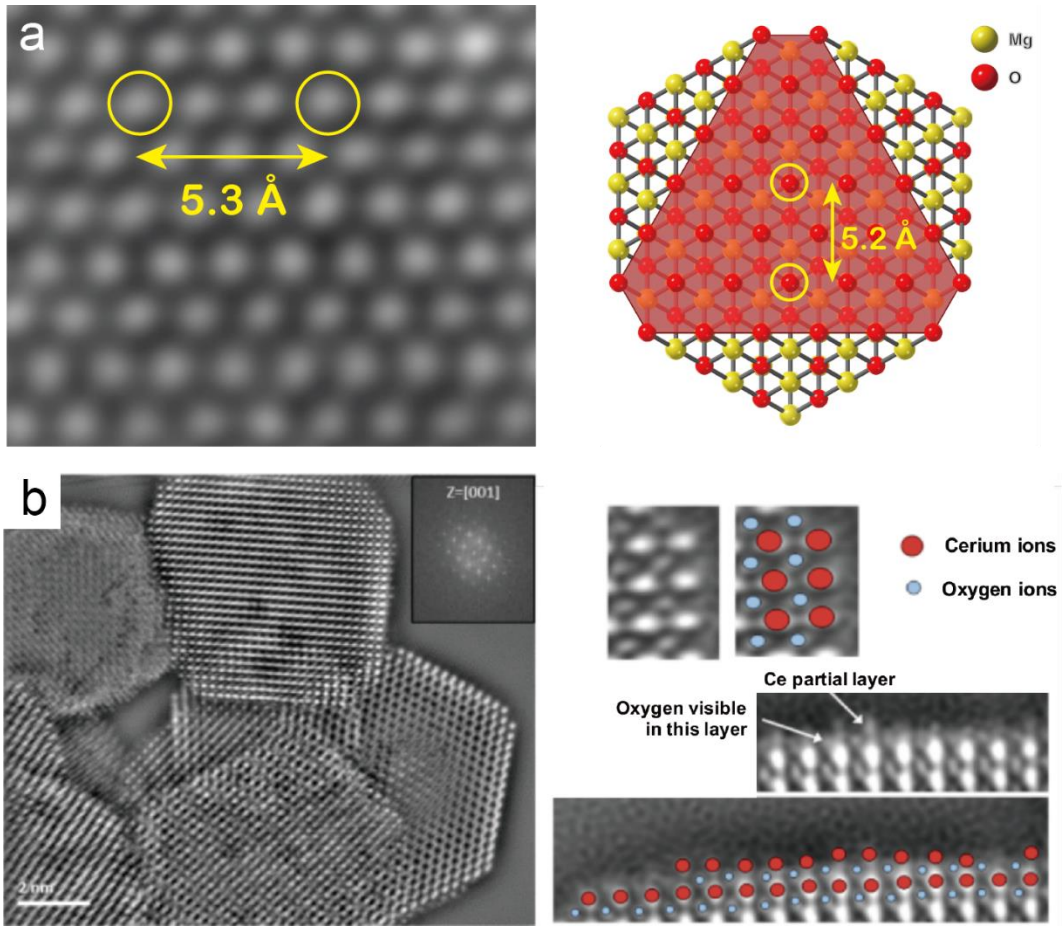

Fig. 2 (a) STEM pattern and simulated model of MgO(111) with exposed O-terminated surface viewed from [111] direction; (b) STEM image of polar CeO_2(100) nanocubes (left) with high magnification of the exit wave restoration (right). Reproduced with permission from ref. 16. Copyright 2019 American Chemical Society.

Such unusual properties lead to extensive efforts on sculpturing the morphology of the nanomaterials. Also, fabrication of high-energy facets' exposure without significant surface

reconstruction (Fig. 2) can be achieved by using appropriate surface directing agents (SDAs), which can influence either the relative surface energies or the facet growth kinetics.[17,18] Catalytic behaviors on different exposed facets have been investigated as well.[4] Here in this review, we focus on the facet-controlled binary metal oxides including MgO, ZnO, TiO_2 and CeO_2 with their nominal cations of increasing redox properties based on our own work. It is aimed to demonstrate that different relaxation processes of their higher energetic facets particularly the polar surfaces, depending on their redox properties, lead to different unique catalytic properties. A range of conventional and novel analytical techniques in identifying unique surface features and exploring structure-activity correlations is also given. Finally, a conclusion of the challenges and future perspectives in this area is also summarized.

2. Case studies

2.1 Hydrogen spillover on polar-faceted MgO surface

MgO has been extensively studied due to its importance in ammonia synthesis, and it is noted the Cs-Ru/MgO configuration has been commercially used as one of the best industrial catalytic systems in Kellogg process at relatively low pressure.[1] Comparing with the conventional large-scale ammonia production via Haber-Bosch process operated at extremely high pressure and temperature (>500 ºC and 25 MPa), ammonia synthesis at mild conditions is attracting more interest. However, it is challenging to achieve at low temperature due to the unfavorable kinetics and the large dissociation energy of the dinitrogen triple bond (941 kJ/mol).[1] Studies were therefore carried out in our group to reveal the underlying principles of the Cs-Ru/MgO catalyst in ammonia synthesis, and unprecedent findings were reported recently.[1]

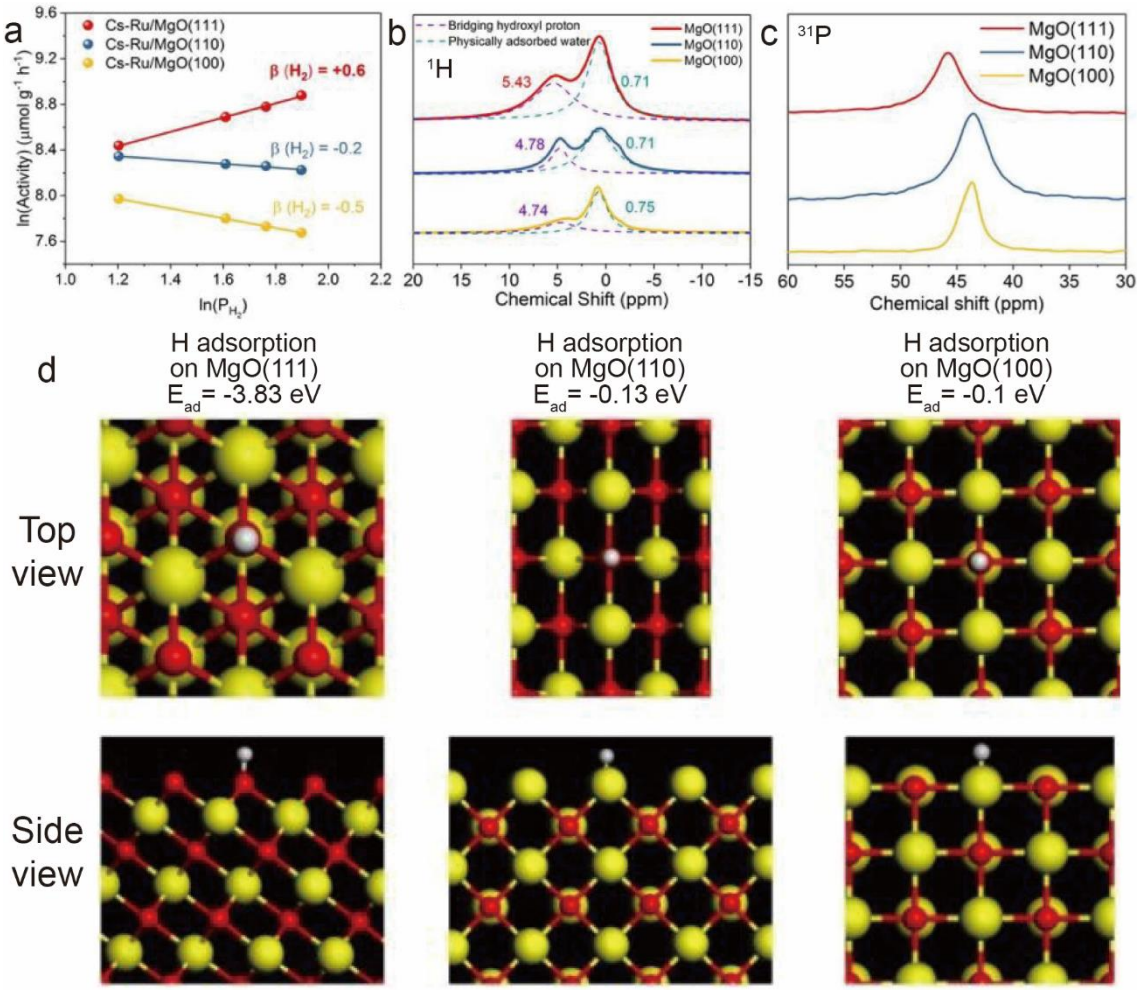

Fig. 3. (a) Dependence of ammonia synthesis rate of Cs-promoted Ru supported on MgO(111), MgO(110), and MgO(100) on H_2 at 643 K; (b) ^{1}H ssNMR, (c) TMPO-assisted ^{31}P ssNMR spectra of MgO(111), MgO(110), and MgO(100); (d) Schematic illustrations of molecular interaction and calculated adsorption energy from DFT between H and O atoms on various MgO surfaces (Mg: yellow; O: red; H: white). Reproduced with permission from ref. 1. Copyright 2020 American Chemical Society.

MgO nanocrystals with preferentially exposed facets of (111), (110) and (100) were fabricated and denoted as MgO(111), MgO(110) and MgO(100), respectively. Interestingly, the Ru/MgO(111)

with preferentially exposed polar O- or Mg-terminated facets without surface reconstruction shows a stable and record-high activity in ammonia synthesis (Fig. 2a and Fig. 3a), as compared with the non-polar counterparts, giving an activity of 4.5 times as high as the commercial MgO catalyst. Notably, the activity differences become more pronounced as hydrogen partial pressure increases (when H_2:N_2 =3.5:1). It should be noted that supported Ru nanoparticles are easily prone to hydrogen poisoning, especially at high hydrogen partial pressures, and typical hydrogen rate order for the ammonia synthesis over traditional Cs-Ru/MgO is around -1,[19] which normally makes high hydrogen partial pressure unfavorable in such system. However, kinetic studies showed that polar-MgO(111) gives a H_2 reaction order of +0.6 at 643K, while in the cases of non-polar supports, the values are negative (Fig. 3a), indicating a rapid hydrogen migration from Ru to MgO(111) so Ru is more receptive for N_2 kinetically. Also noteworthy is the non-redox properties of Mg^{2+} hinder MgO from surface oxygen vacancy (V_o) formations and oxidation state changes due to the exceptionally high ionization energy (ca. 1451 $kJmol^{-1}$). As a result, the strong surface polarity of this (111) facet remains, which exerts remarkable interactions with the chemical species nearby. We recently reported that the surface polarities can be investigated by ssNMR technique using trimethylphosphine (TMP) or trimethylphosphine oxide (TMPO) as surface probes (details about the probe-assisted ssNMR are shown in the Supporting Information). As shown in Figs. 3b and 3c, ^{1}H MAS NMR and ^{31}P ssNMR using trimethylphosphine oxide (TMPO) as probe confirmed the superior affinity of H on the polar MgO(111) surface, given that large changes of the chemical shift values were directly observed on both ^{1}H and ^{31}P spectra. Such observation was supported by FT-IR.[1] Operando AP-XPS, on the other hand, shed light on the coverage and the depth that the surface H can travel. DFT calculations reveal the adsorption energy of H on O-terminated (111) facet (3.83 eV) is more than 10 times higher than those on the non-polar (110) and (100) (< 0.3

eV) (Fig. 3d), thus resulting in a high affinity of support to mob up hydrogen from Ru. The local electric field (LEF) introduced by the polar MgO (111) surface facilitates the adsorption of proton and provides the driving force for the adsorbed H species to migrate from the Ru surface to the O^{2-} sites and hop on the polar support. Thus, the use of MgO(111) support with the dominant polar surface works as a more efficient catalyst promotor for ammonia synthesis than those with non-polar surfaces.[1]

2.2 LEF for exciton lifetime extension by polar-faceted metal oxides in photocatalysis

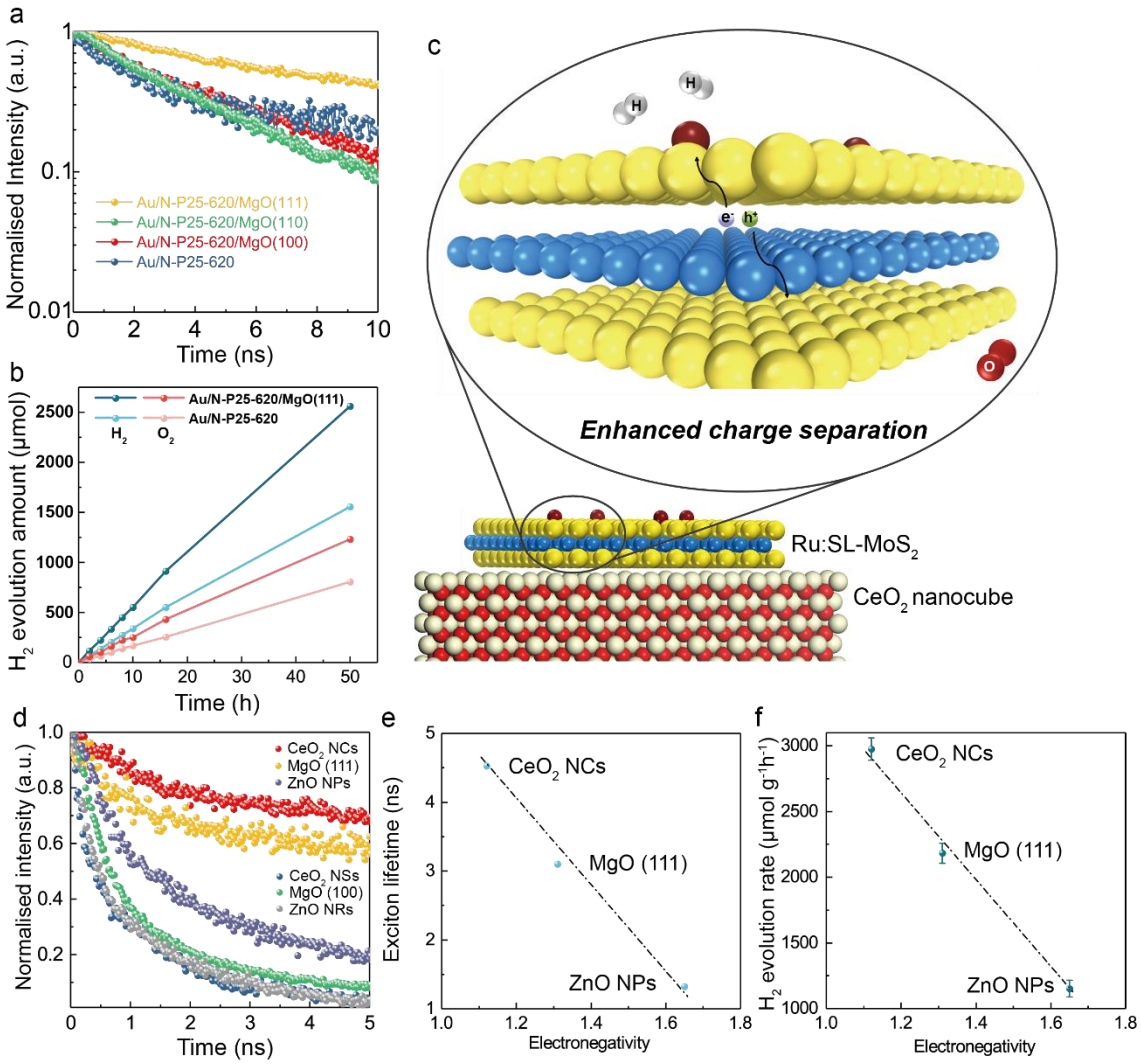

Fig. 4. (a) TRPL spectra of Au/N-P25-620 mixed with different MgO supports; (b) Stoichiometric decomposition of pure water over Au/N-P25-620 with and without MgO (111); Reproduced with permission from ref. 3. Copyright 2019 Springer Nature. Distributed under a Creative Commons Attribution License 4.0 (CC BY) https://creativecommons.org/licenses/by/4.0/; (c) Schematic illustration of the LEF effect on doped MoS_2 monolayers introduced by polar-faceted CeO_2 nanocubes; (d) TRPL spectra of Ru:SL-MoS_2 after mixed with various supports; (e) exciton lifetimes and (f) photocatalytic H_2 evolution rates of Ru:SL-MoS_2 in a linear relationship with the polarization introduced by polar-faceted oxides. Reproduced with permission from ref. 20. Copyright 2020 Elsevier.

Further investigation was then moved to photocatalytic overall water splitting (POWS) reaction, which is of importance for solar energy storage in the form of H_2. However, no practical application has been realized so far, due to the poor activity and quantum efficiency (QE) arisen from the fast charge recombination. We recently demonstrated that extraordinary POWS activity and QEs can be achieved at elevated temperatures over N-doped TiO_2 (N-TiO_2) on polar oxide supports under visible light irradiation (more information of photocatalysis at elevated temperatures is shown in Supporting Information).[3] It is due to the fact that strong LEF can be generated near the polar surfaces.[15] In spite of the relaxation processes which lower the surface polarity,[21] the rigidity of the metal oxides still hampers such processes to a large extent and leaves considerable polarity and electrostatic forces on the polar surfaces. MgO with polar (111) facets, which has been discussed before, was initially engaged as the support for the Au/N-TiO_2 photocatalyst. Time-resolved photoluminescence (TRPL) measurements were carried out, showing that MgO (111) remarkably prolonged the exciton lifetime of N-TiO_2, while the non-

polar MgO (100) and MgO (110) showed no such influence (Fig. 4a). The photocatalytic activity of the MgO (111) promoted Au/N-TiO_2 gave an unprecedented hydrogen evolution rate of 11092 μmol $g^{-1}h^{-1}$ at 270 ºC, whereas non-polar MgO (100) or (110) showed no promotion in rate at all (Fig. 4b).[3] Extraordinary QEs of 81.8% at 437 nm and 3.2% at 1000 nm were also achieved with the inclusion of MgO (111). The use of polar-faceted MgO(111) can introduce an LEF, which prolongs the exciton lifetimes and therefore enhances the photocatalytic water splitting activities. Subsequently, other polar-faceted oxides such as CeO_2 nanocubes and ZnO nanoplates were also used to study the LEF effect, which showed similar behavior as the MgO (111), whereas their non-polar counterparts barely show any effect.[3] Our recent results also indicate that the polar-faceted supports exert similar effects on the monolayer MoS_2, as illustrated in Fig. 4c.[20] By using TRPL, it is demonstrated that the photocatalytic activities and exciton lifetimes were correlated well with the LEF strengths (polarity calculated from the difference in electronegativity), hence giving apparent linear relationships (Figs. 4d-f).

2.3 SMSI on the polar surface of faceted ZnO

It is widely accepted that ZnO is composed of tetrahedrally coordinated O^{2-} and Zn^{2+} ions stacking along the c-axis, which means there are a positively charged Zn-terminated (002) facet (Zn-(002)), a negatively charged O-terminated (002) facet (O-(002)) and nonpolar (100) facets with C_{6V} symmetry, as shown in Fig. 5a.[22,23] The exposure of the (100) and (002) facets can be tuned by controlling the length and diameter of the hexagonal structure.

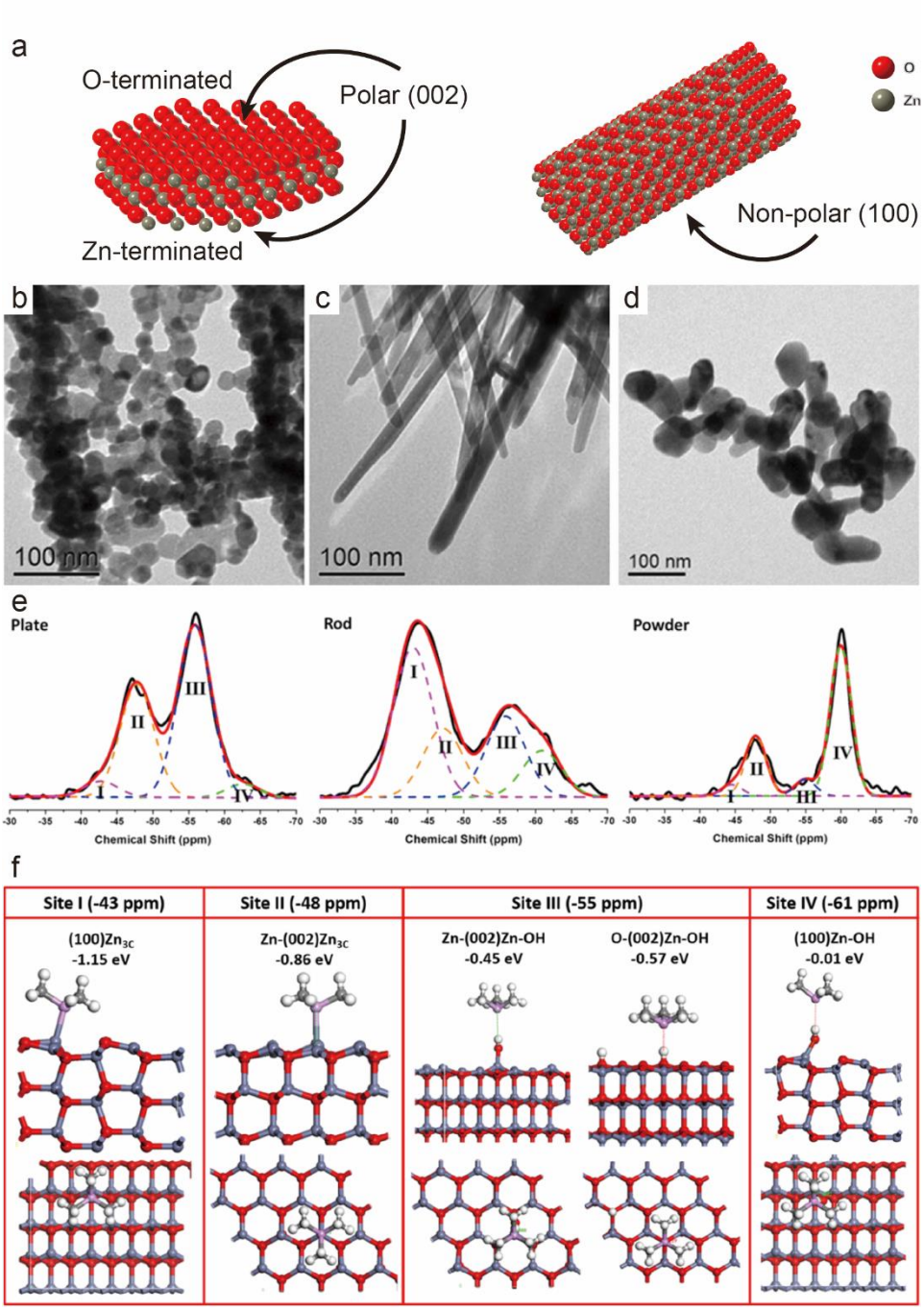

Fig. 5. (a) Models of ZnO morphologies and exposed facets; (b-d) TEM of ZnO nanoplates, nanorods and powders. Reproduced with permission from ref. 24. Copyright 2016 Wiley-VCH. (e) TMP-assisted ^{31}P ssNMR spectra of ZnO nanostructures; (f) Calculated structures of TMP

adsorbed on different sites of ZnO. Reproduced with permission from ref. 4. Copyright 2016 American Chemical Society.

We have reported a controlled synthesis of ZnO nanocrystals with different morphologies, including nanoplates with preferentially exposed polar (002) facets, the nanorods with dominant exposure of non-polar (100) facets and amorphous powders (Figs. 5b-5d).[24–26] Cu NPs were then synthesized and mixed with the SDA-free ZnO nanostructures to investigate the interaction and the interfaces between ZnO and Cu NPs. Catalytic performances of the different morphologies were then carefully studied in CO_2 hydrogenation for methanol production. Table 1 clearly shows that Cu/ZnO nanoplates exhibited higher selectivity to methanol in CO_2 hydrogenation reaction, reaching over 70%.[26] To reveal the underlying principles of the superior catalytic performances of the polar ZnO nanoplates, various characterization techniques were utilized. XPS shows that the O 1s binding energy (BE) of the polar facets changes a lot after addition of Cu NPs, while that of non-polar facets remains constant, suggesting that there are strong electron transfers between Cu NPs and polar (002) facet, described as 'strong metal support interaction' (SMSI) at the interface[26]. EPR spectra showed that two intense signals at g=2.00 and g=1.96 were observed for polar ZnO nanoplates, whereas only the signal at g=2.00 with much lower intensity was detected for the non-polar nanorods. The former signal is usually attributed to the deeply trapped electrons in V_o, and the signal at g=1.96 derives from the shallow trapped single electrons in the conduction band (CB).[27] Quantitative analysis indicated ZnO nanoplates possess much more V_o than the nanorods. The more favorable formation of surface V_o due to relaxation of polar ZnO surface (difference in 2^{nd} to 1^{st} IE = 826 kJ mol^{-1}) may create active sites for H_2 activation as well as Cu species interactions. Further EPR measurements also showed the electrons originally trapped in the CB of

ZnO nanoplates of lower energy (see Fig. 1) can transfer to the Fermi level of Cu NPs, while no such behaviors could be observed on the non-polar nanorods. The temperature-programmed reduction (TPR) analysis showed the facilitated oxygen reduction in the interface of Cu NPs and polar ZnO nanoplates, which could subsequently contribute to the activation of CO_2 molecules. Subsequently, ssNMR using trimethylphosphine (TMP) as a surface probe was carried out for the ZnO nanomaterials and deconvoluted into four components, as shown in Fig. 5e, and the concentration of each site can be quantified according to the peak area.[4] DFT calculations in Fig. 5f clearly indicates that the NMR signals of Site I and Site II are attributed to the interaction of TMP with unsaturated three-coordinate Zn (Zn_{3C}) on (100) and (002) facet, respectively. Besides, the interaction between the protons of surface OH groups (Brϕnsted acid sites) and TMP was found highly dependent on the surface polarity of the ZnO facets (Site III and Site IV). Clearly, the Lewis acid (LA) sites of polar (002) facets showed stronger LA acidities (Site II and Site III), which led to the preferential adsorption of molecules on the polar facet and such phenomenon could be attributed to the difference of intrinsic surface energy between facets.[4] In addition, the high energetic and instability of the ZnO nanoplates originated from the exposure of polar surface could also lead to enhanced V_o formation due to charge transfer from this surface to active metal component. All the unique properties result in a stronger SMSI of ZnO nanoplates with the overlying metallic NPs, hence lead to improved catalytic activities.

Table 1. Catalytic performance of ZnO nanoplates and nanorods in the synthesis of methanol from hydrogenation of CO2. [a] 26

CO_2:H_2 molar ratio	T (K)	Catalyst	CO_2 conversion (%)	Methanol selectivity (%)

1:2.2	543	ZnO nanorods	12.3	42.3
		ZnO nanoplates	10.9	72.7
	553	ZnO nanorods	15.3	39.1
		ZnO nanoplates	12.0	71.6
1:2.5	543	ZnO nanorods	15.8	41.0
		ZnO nanoplates	15.5	64.5
	553	ZnO nanorods	17.8	32.0
		ZnO nanoplates	14.7	63.3

[a] Flow rate: 40 stp mL min^{-1} at 4.5 MPa. Catalyst was mixed with Cu and Al_2O_3

2.4 Adsorbed impurities on faceted TiO_2

Anatase TiO_2 has been attracting versatile applications including hydrogen evolution, water splitting, dye-sensitized solar cells, etc.[28] The synthetic TiO_2 nanocrystals are generally covered with the thermodynamically favorable and less active (101) facet rather than the active (001) facet.[29,30] Although (001) facet is not a polar surface, it is a more energetic than (101). Fluorine was reported to be able to change the relative growth rates as an SDA, resulting in preferential exposure of (001) facet,[31] however, the complete removal of fluorine is an issue, whose effects have long been underestimated. Calcination and aqueous NaOH wash are mostly used in post-treatments to obtain so-called clean surface. However, different removal methods always result in diverse or even contradicting results in literature, leading to different interpretations and frequent disagreements among researchers.[32]

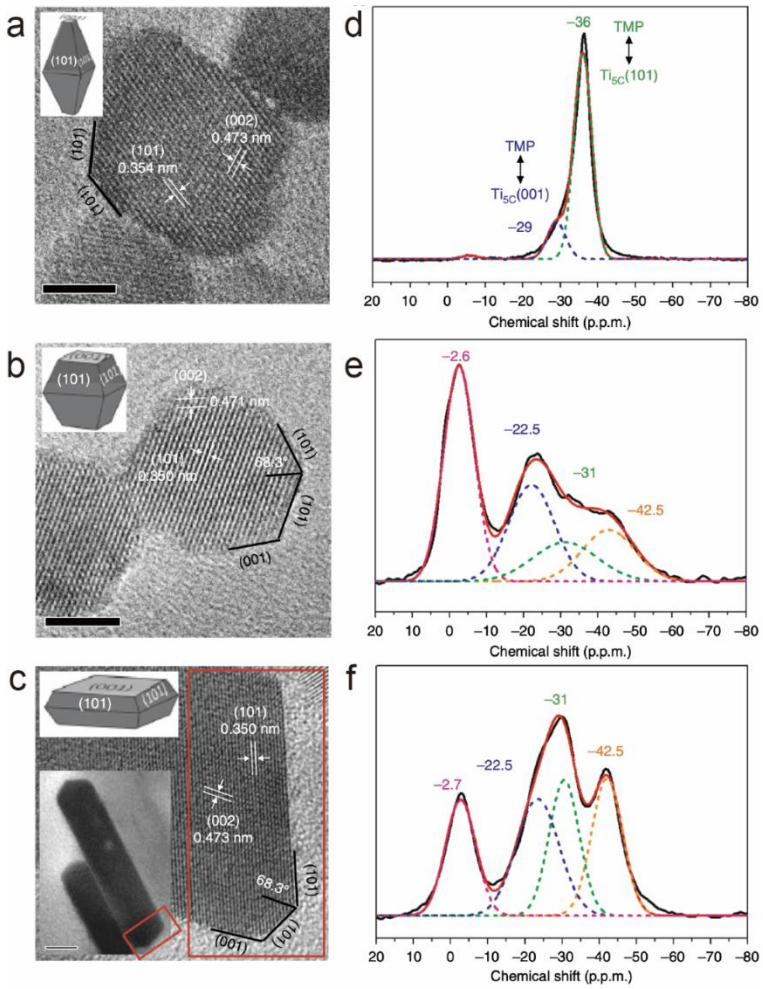

Fig. 6. TEM images (a-c) and ^{31}P ssNMR spectra (d-f) of TiO_2 PD, F-(101) and F-(001), respectively. The scale bars are 5 nm. Reproduced with permission from ref. 32. Copyright 2017 Springer Nature. Distributed under a Creative Commons Attribution License 4.0 (CC BY) https://creativecommons.org/licenses/by/4.0/.

Consequently, high quality anatase TiO_2 nanocrystals with different exposed facets were fabricated by our group using hydrothermal synthesis, labelled as TiO_2 powder (PD), F-(101) and F-(001), as shown in Figs. 6a-6c.[32] The percentages of the (001) facet exposure of the PD, F-(101) and F-(001) samples were estimated to be 10.2%, 21.1% and 75.4%, based on the Wulff

construction model.[5] Unlike the case of ZnO where surface relaxation creates M^+ (Zn^{2+} + e-) and V_o, lower formation energy of sub-surface V_o than surface V_o and fast oxygen mobility [33] cause surface Ti-O to retain Ti-F-(OH), resulting in considerable change of the local electronic environment. Probe-assisted ^{31}P ssNMR was used to investigate the surface features, which showed very different spectra (Figs. 6d-6f). The F-stabilization on the (001) and (101) facets can largely enhance the LA strength of five-coordinate Ti (Ti_{5C}) by showing downshift of $\delta^{31}P$. The post-calcination was shown to partially replace F with OH group, rendering the upshifts of $\delta^{31}P$, which means the LA strength of Ti_{5C} is reduced. The high-energy (001) facets tend to adsorb different surface impurities groups to relax their energy and they exert substantial effects on the surface LA strengths which subsequently influence the photocatalytic activities.

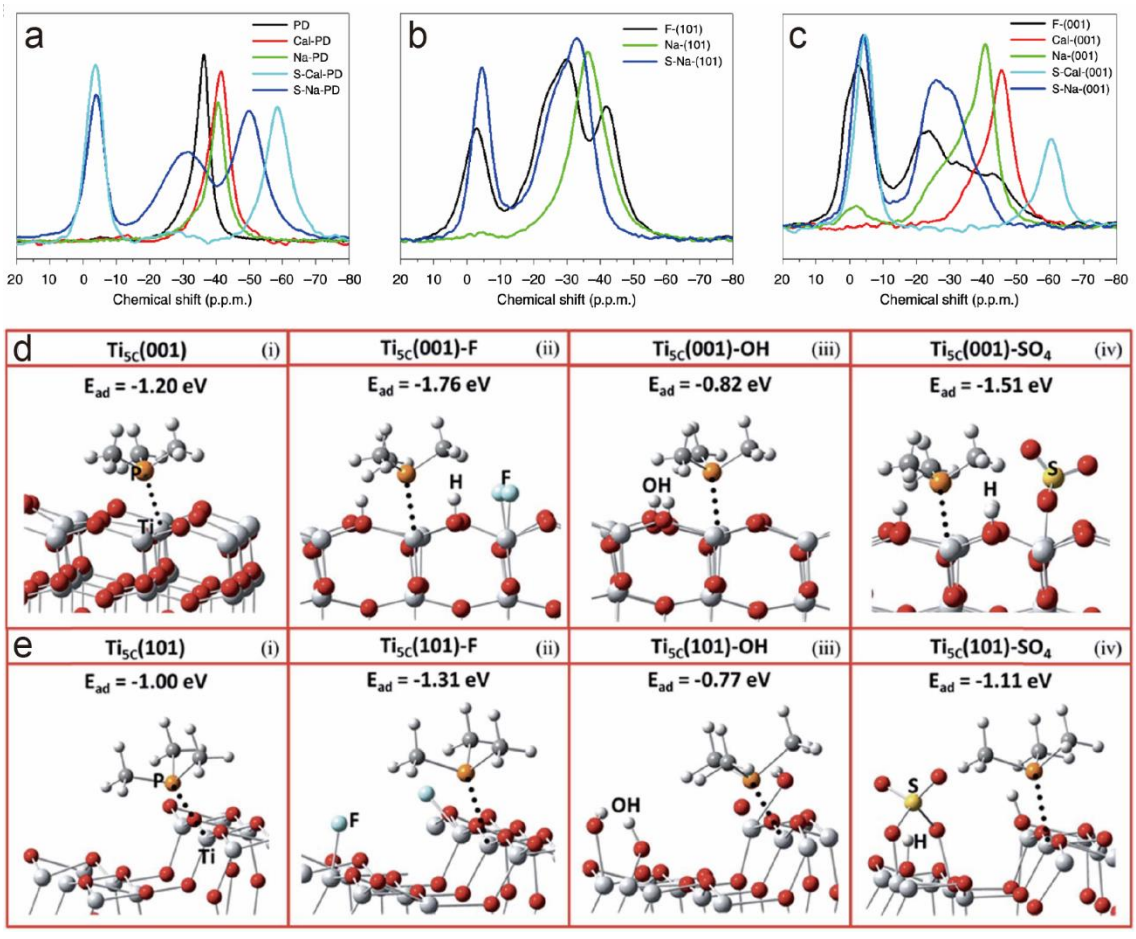

Fig. 7. TMP-assisted 31P ssNMR spectra of TiO2 (a) PD, (b) F-(101) and (c) F-(001) after different surface treatments. Reproduced with permission from ref. 32. Copyright 2017 Springer Nature. Distributed under a Creative Commons Attribution License 4.0 (CC BY) https://creativecommons.org/licenses/by/4.0/; Schematic illustrations of the TMP adsorption on (d) (001) and (e) (101) facets with different surface groups. Reproduced with permission from ref. 5. Copyright 2018 Royal Society of Chemistry. Distributed under a Creative Commons Attribution 3.0 Unported License (CC BY) https://creativecommons.org/licenses/by/3.0/.

A separate study also shows the local surface features play the key role in photocatalytic HER[34]. It was observed by ssNMR that the electron density of surface Ti_{5C} is largely decreased in the presence of F. TRPL was used to evaluate the influence on the charge separation process, which showed the exciton lifetimes were prolonged with higher concentration of surface F groups. Therefore, surface F groups can largely influence the local electronic properties and trap the photo-generated electrons due to its strongest electronegativity, which consequently suppress the charge carrier recombination and leads to enhanced photocatalytic activities. Such point was further investigated by using other surface functional groups (i.e. OH and SO_4), which were systematically studied by ssNMR and DFT. The NMR spectra vary greatly depending on the surface electronic states for each sample (Figs. 7a-7c) and different adsorption geometries were elucidated by DFT calculations (Figs. 7d and 7e). For each situation, the adsorption on F-(001) is much stronger than that on F-(101). Moreover, the adsorption energies on surfaces modified by different groups show a linear relationship with the $\delta^{31}P$ on ssNMR and the photocatalytic HER activities .[5] Clearly, the surface impurities can change the electron densities of the nearby Ti_{5c} sites, which further influence the photo-generated charge carriers' separation and the photocatalytic performances.

2.5 Fast redox change of faceted CeO_2 nanomaterials

CeO_2 has been extensively studied as an active redox catalyst, catalyst promoter or support with metal promotor in catalysis and electrocatalysis,[16,35] due to high oxygen storage, fast surface oxygen mobility, and so forth,[36] which could exhibit SMSI with the overlying metal NPs.[37–39] Different from the above discussed MgO, ZnO and TiO_2, a much larger quantity of oxygen can be extracted from CeO_2 well beyond surface by easily changing the oxidation state of Ce due to the remarkably fast Ce^{4+}/Ce^{3+} redox cycle in couple with the added metal promotor. Thus, the surface interaction of metal and Ce^{4+}/Ce^{3+} redox pair at the specific facets can exert stronger effects on catalytic performances.

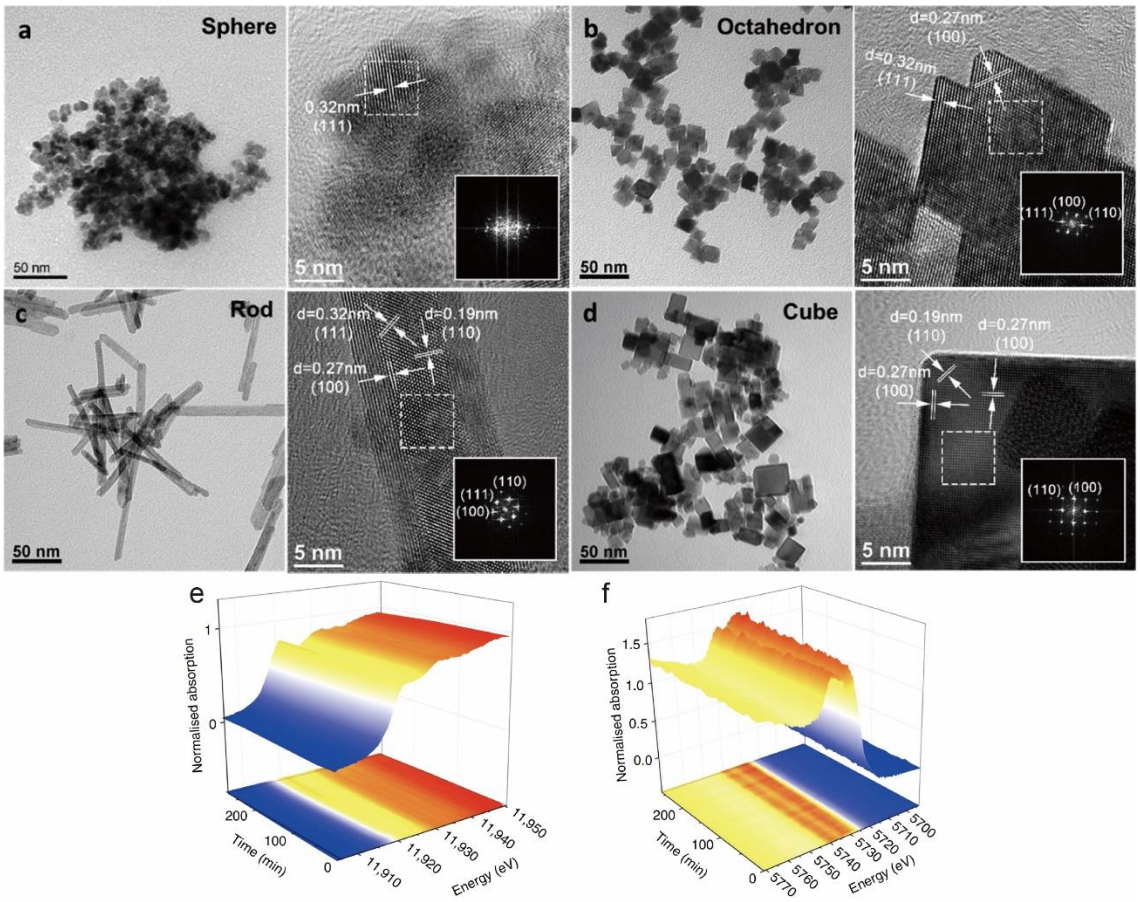

Fig. 8. TEM images of the CeO2 (a) nanospheres, (b) octahedrons, (c) nanorods, and (d) nanocubes. Reproduced with permission from ref. 40. Copyright 2020 American Chemical Society. In-situ XANES spectra of (e) Au L3 edges and (f) Ce L3 edges as a function of reaction time. Reproduced with permission from ref. 2. Copyright 2019 Springer Nature. Distributed under a Creative Commons Attribution License 4.0 (CC BY) https://creativecommons.org/licenses/by/4.0/

CeO_2 nanocrystals with different morphologies were studied by our group.[2,16,35,40] Microscopic techniques show the amorphous nanospheres, octahedron with exposed (111) facets, nanorods with non-polar (110) facets and the nanocubes with preferentially exposed polar (100) facets (Figs. 8a-8d). The CeO_2 nanorods with (110) facet is proved to be a good catalytic component for non-reduction or oxidation reactions such as acetylene hydrochlorination reaction for the synthesis of vinyl chloride monomer (VCM).[2] After inclusion CeO_2 nanorods in the Au/activated carbon (AC) catalyst, the catalyst showed superior and stable activity for more than 3000 h (125 days) without deactivation, whereas Au/AC progressively deactivated within 500 h.[2] This Au/CeO_2&AC catalyst even shows the ability of self-regeneration. It is generally believed that the Au(III)/Au(I) pairs act as active sites of the VCM production over Au/AC catalyst, and Au aggregation occurs when the Au(I) and Au(III) species are over-reduced to Au(0). The catalysts were thus investigated by X-ray absorption near edge structure (XANES) spectroscopy (Figs. 8e and 8f). However, Au(III) species are barely detected in the in-situ XANES, on the contrary, the Au(0) species are found as more than 70%. We also observed the progressive increase of Ce(III) at the expense of Ce(IV), while the simultaneous oxidation process of Au(0) to Au(I) occurs. Such observation indicates that the one electron fast complementary redox coupling reaction between Au(0)/Au(I) and

Ce(IV)/Ce(III) in this composite catalyst plays a dominant role, whereas the redox change of Au(I)/Au(III) would require two one-electron transfer steps from nearby Ce(IV)/Ce(III) sites with anticipated higher activation barriers.[2] Clearly, the surface feature of CeO_2 nanorods with (110) facets not only accommodates and stabilizes Au species but also facilitates a fast changing redox pair of Au(0)/Au(I), resulting in the superior activity and the unique self-regeneration feature.[2]

2.6 Fast oxygen mobility of faceted CeO_2 nanomaterials

On the other hand, Pd/CeO_2 nanocubes with dominant polar (100) facet exposure shows at least 2 times higher activity than the other non-polar CeO_2 samples in (electro)catalytic reactions, which also appears to be less susceptible to CO poisoning.[16] Operando ambient pressure (AP) XPS showed that in Pd/CeO_2 nanocubes, the Ce^{3+}/Ce^{4+} ratio was maintained at around 0.3 regardless of whether in reduction or oxidation environments, and the conversion between Pd(0) and Pd(II) was also suppressed, suggesting the high oxygen mobility of polar CeO_2 and fast Ce^{4+}/Ce^{3+} redox pair can resist the change of oxidation states in overlying metal.[16] More detailed study of the Pd/CeO_2 nanocubes system was then performed with the help of electron energy loss spectroscopy (EELS). Three consecutive EELS Ce^{4+} mappings of Pd/CeO_2 nanocubes are shown in Fig. 9a, which clearly indicate after the 1st scan, the reduction of Ce^{4+} to Ce^{3+} goes deeper beyond the surface layer. The Pd mappings are shown in Fig. 9b, while a HAADF-STEM image is given in Fig. 9c. Then the rates of reduction between subsequent scans were calculated and mapped, which are represented by different colors in Fig. 9d. Apparently, the deeper extensive regions of CeO_2 nanocubes experienced faster rate of reduction. The fastest reduction rates occurred at the CeO_2-Pd interfaces, where nearly all the Ce^{4+} had been reduced to Ce^{3+} at the region around the Pd even before the 1st scan was taken. Noticeably, Pd/CeO_2 nanorods and CeO_2 nanocubes without Pd

were also studied and showed no such behaviors (Figs. 9e-9h).[35] The effects arisen from the Ce^{4+}/Ce^{3+} redox pair was also supported by the TMP probe-assisted ssNMR measurements.[40] The CeO_2 nanocubes (100), nanorods (110), octahedron (111) and nanospheres (amorphous) showed very different ^{31}P NMR spectra, indicating the chemical environment of surface Ce species is highly facet-dependent. The facet-dependent LA acidity decreases as (111)> (110)> (100), derived from $\delta^{31}P$ values, which is attributed to the increasing Ce^{3+} concentrations among these facets.[40] Thus, the fast Ce^{4+}/Ce^{3+} redox cycle coupled with unique oxygen hopping involving both surface and sub-surface oxygen of polar CeO_2 (111) play a key role in the catalytic performances of faceted CeO_2 for reduction and oxidation processes.[41]

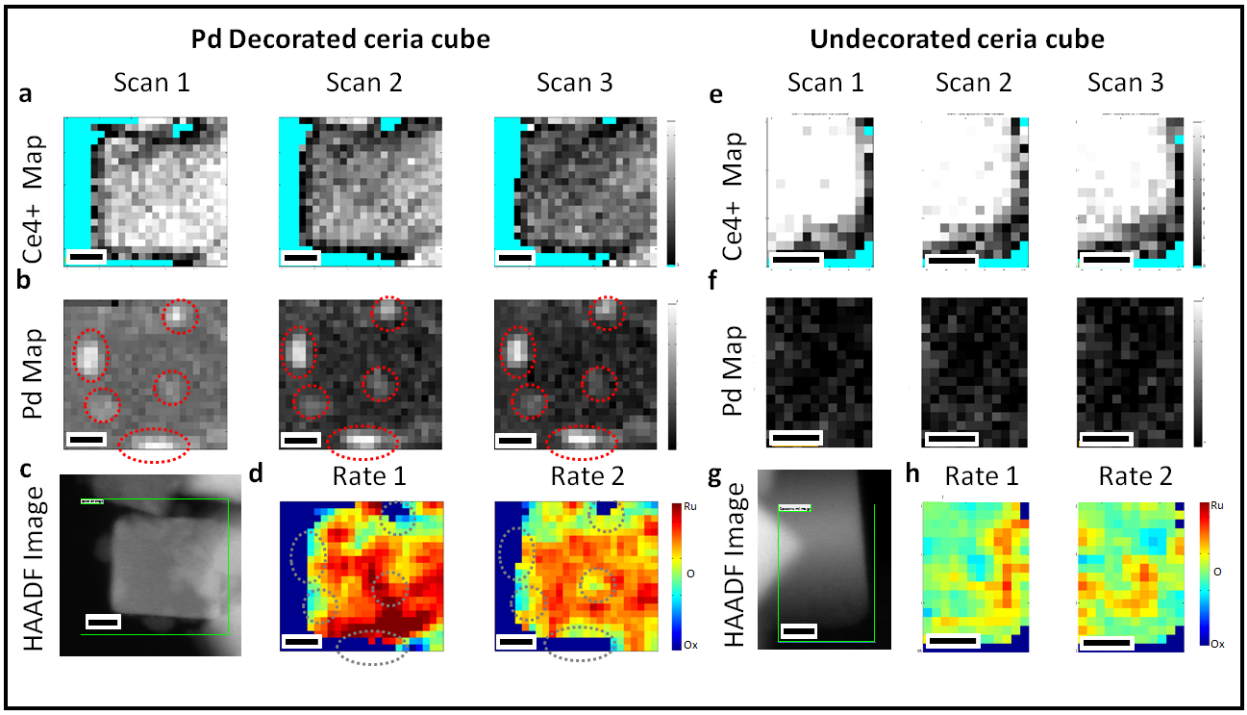

Fig. 9. Compositional EELS mapping of 1% Pd/CeO_2 nanocubes and pure CeO_2 nanocubes. (a) and (e) The Ce^{4+} mapping after 1st, 2nd and 3rd STEM-EELS scans; (b) and (f) Pd mapping with the position of Pd particles marked with red dotted circles; (c) and (g) STEM HAADF images; (d) and (h) The rate of reduction between subsequent scans (represented by the visible light spectrum

colors). All the scale bars are 5 nm. Reproduced with permission from ref. 35. Copyright 2020 Elsevier. Distributed under a Creative Commons Attribution License 4.0 (CC BY) https://creativecommons.org/licenses/by/4.0/

3 Other faceted materials

Other energetic faceted materials were also studied by our group, such as pseudo-hexagonal TT Nb_2O_5 nanorods with preferentially exposed (100) facets [42] and β-Ga_2O_3-based nanomaterials [43,44]. Other materials that can become polar upon external excitation by photo, electrical or piezometric means still lack of in-depth investigation. For example, ferroelectric materials including 2D InSe and $CuInP_2S_6$ monolayers and 3-D ternary $BiFeO_3$ perovskite show strong induced polarity upon photo-irradiation.[45–47] As is well known, layered dichalcogenide MoS_2 can be chemically exfoliated into single/multi-layered nanosheets leading to enhanced exposure of the polar S-terminated surface.[48] Apparently, the specific polar facets of the layered materials can also be easily obtained via top-down approach. Generally, surface S-vacancies are created during the chemical exfoliation, which serve as surface anchoring sites for metal atoms or clusters. Our study demonstrated that cobalt single atoms can be dispersed onto the exfoliated monolayer MoS_2 via this defect engineering.[48] The resulted material is extremely active, selective and stable for the conversion of 4-methylphenol to toluene in hydrogen, which opens the possibility of using this novel type of catalysts for biomass conversion. The single atom doped polar MoS_2 monolayers were also found to exhibit promising performances in HER and PEM electrolyzer.[49–51] Likewise, unique properties are observed on using layered double hydroxides (LDHs), which are well-defined materials with polar layered structures along their main crystallographic [100] direction.

Very recent results show that their strong local polarity facilitates charge separation process, leading to enhanced photocatalytic activities toward water splitting reaction.[19]

4 Summary and perspectives

It is accepted that engineered exposure of specific facets of catalyst or support, especially the high-energy polar surfaces provide an excitingly new strategy in rational design of heterogeneous catalysts. Using various SDAs, one can tailor the exposed facet during the nanocatalysts synthesis. In our research, metallic NPs, metal oxides and other related materials have been extensively studied for their unique surface properties and the correlation with catalytic performances. The unusual properties of polar surfaces in catalysis arise from the high surface energy, unique ion distribution to give rise to local polarity and bandgap reduction as summarized in Fig. 1. However, the precise route for relaxation of this high energetic facet is highly dependent on many factors. For example, non-reducible metal cations in metal oxides such as MgO(111) with difficulties of relaxation exert persistent strong local polarization which can affect local charge distribution (exciton produced from photocatalyst). The O-terminated facet gives high affinity of counter-ions such as protons, hence resulting in hydrogen spillover phenomenon. For polar metal oxide with cation that can undergo redox change at relatively low energy, formation of oxygen vacancies and Zn^{+} can take place as a way to relax the surface energy. Such pathway can alter bandgap and change surface oxygen vacancy concentration, which gives unique SMSI with overlying NPs. In polar CeO_2 (100) facets, facile oxidation state change of Ce in reductive environment to relax the surface energy allows deep access to oxygen, giving a remarkable performance for reduction-oxidation reactions.[16]

Clearly, further exploration of polar facet effects is important. However, one should be very cautious about possible surface reconstruction of this energetic facet especially during the removal of SDAs and their studies under extreme conditions. Also, the surface area of different nanostructures should be well-controlled by modifying the synthesis conditions in order to fairly compare the polarization effect on different exposed facets. Besides, in the cases where overlying metallic NPs are included, the mean size of the NPs on different polar and non-polar surfaces should also be controlled as the same. The confirmation of polar facet and surface structure before and after catalysis must be ensured before any correlation to catalytic activity. In addition, it should be noted that the catalysis can be influenced by various factors, therefore, multiple structural and electronic features on the facet upon relaxation may require careful differentiation and assessment in order to identify the main reason for modulating catalytic activity. We will no doubt require more powerful analytical tools especially those operando/in-situ techniques. Apart from traditional characterizations like XPS and microscopy, we showed the powerful collective uses of EPR, TRPL, AP-XPS, XANES and probe-assisted ssNMR under different circumstances. In particular, the ssNMR exhibits remarkable ability of differentiating facets and identifying the surface states. With the help of such techniques, we elucidated the electronic/geometric properties such as surface LA sites, nature of functional groups, surface defects, charge transfer process, etc. These studies lead to better understandings of the specific roles that polar facet plays, hence lead to establishment of structure-activity correlations. It is also noteworthy that the above-mentioned metal-oxide-based catalysts show great stability or self-regeneration ability toward different catalytic reactions, meanwhile, the binary metal oxides are cheap and abundant, which makes the polar-faceted metal oxides quite promising to further practical applications. We believe such materials are suitable for

lab-scale model systems and with a good potential to find large-scale applications (see Supporting Information).

The present analytical tools are still insufficient. For example, the quantification of local electric field introduced by polar-faceted materials should be achieved, which may contribute to wider applications of the facet-engineering techniques for solar energy conversion technologies.[3] Investigation of 2-D layer-structured composites can also be a novel direction for fabricating specific exposed polar facets of variable strengths, which requires new tools to correlate local field strength with catalysis.

AUTHOR INFORMATION

Corresponding Author

*Shik Chi Edman Tsang: edman.tsang@chem.ox.ac.uk

Author Contributions

This review is written jointly by Yiyang Li and Shik Chi Edman Tsang.

Biographies

Yiyang Li received a BSc in chemistry at Fudan University in 2017. Currently, he is studying his DPhil at the University of Oxford, UK.

Shik Chi Edman Tsang is a professor of Chemistry and the Head of the Wolfson Catalysis Centre at the University of Oxford, UK. He has particular expertise in the design of nanocatalysts, which can lead to the understanding of catalytic surfaces and interfaces.

Note

Supporting Information including more details of photocatalysis at elevated temperatures and ssNMR technique is available for this article.

REFERENCES

(1) Wu, S.; Peng, Y.-K.; Large, A. I.; Zheng, J.; Chen, T.; Duan, H.; McPherson, I. J.; Wilkinson, I.; Chou, H.-L.; Held, G.; Tsang, S. C. E. Removal of Hydrogen Poisoning by Polar MgO Support for Low Pressure NH3 Synthesis at Unprecedented Rate over Ru Catalyst. *ACS Catal.* **2020**, *10*, 5614–5622. https://doi.org/10.1021/acscatal.0c00954.

(2) Ye, L.; Duan, X.; Wu, S.; Wu, T. S.; Zhao, Y.; Robertson, A. W.; Chou, H. L.; Zheng, J.; Ayvalı, T.; Day, S.; Tang, C.; Soo, Y. L.; Yuan, Y.; Tsang, S. C. E. Self- Regeneration of Au/CeO2 Based Catalysts with Enhanced Activity and Ultra-Stability for Acetylene Hydrochlorination. *Nat. Commun.* **2019**, *10*, 914. https://doi.org/10.1038/s41467-019-08827-5.

(3) Li, Y.; Peng, Y.-K.; Hu, L.; Zheng, J.; Prabhakaran, D.; Wu, S.; Puchtler, T. J.; Li, M.; Wong, K.-Y.; Taylor, R. A.; Tsang, S. C. E. Photocatalytic Water Splitting by N-TiO2 on MgO (111) with Exceptional Quantum Efficiencies at Elevated Temperatures. *Nat. Commun.* **2019**, *10*, 4421. https://doi.org/10.1038/s41467-019-12385-1.

(4) Peng, Y. K.; Ye, L.; Qu, J.; Zhang, L.; Fu, Y.; Teixeira, I. F.; McPherson, I. J.; He, H.; Tsang, S. C. E. Trimethylphosphine-Assisted Surface Fingerprinting of Metal Oxide Nanoparticle by 31P Solid-State NMR: A Zinc Oxide Case Study. *J. Am. Chem. Soc.* **2016**, *138*, 2225–2234. https://doi.org/10.1021/jacs.5b12080.

(5) Peng, Y. K.; Chou, H. L.; Edman Tsang, S. C. Differentiating Surface Titanium Chemical States of Anatase TiO_2 Functionalized with Various Groups. *Chem. Sci.* **2018**, *9*, 2493–2500. https://doi.org/10.1039/c7sc04828a.

(6) Von P. A. Cox. *The Electronic Structure and Chemistry of Solids*; 1987. https://doi.org/10.1002/ange.19881000536.

(7) Lee, H. E.; Ahn, H. Y.; Mun, J.; Lee, Y. Y.; Kim, M.; Cho, N. H.; Chang, K.; Kim, W. S.; Rho, J.; Nam, K. T. Amino-Acid- A Nd Peptide-Directed Synthesis of Chiral Plasmonic Gold Nanoparticles. *Nature* **2018**, *556*, 360–365. https://doi.org/10.1038/s41586-018-0034-1.

(8) Tauster, S. J.; Fung, S. C.; Baker, R. T. K.; Horsley, J. A. Strong Interactions in Supported-Metal Catalysts. *Science* **1981**, *211*, 1121–1125. https://doi.org/10.1126/science.211.4487.1121.

(9) Cuenya, B. R. Metal Nanoparticle Catalysts Beginning to Shape-Up. *Acc. Chem. Res.* **2013**, *46*, 1682–1691. https://doi.org/10.1021/ar300226p.

(10) Li, M. M. J.; Tsang, S. C. E. Bimetallic Catalysts for Green Methanol Production via CO2 and Renewable Hydrogen: A Mini-Review and Prospects. *Catal. Sci. Technol.* **2018**, *8*, 3450–3464. https://doi.org/10.1039/c8cy00304a.

(11) Trindell, J. A.; Duan, Z.; Henkelman, G.; Crooks, R. M. Well-Defined Nanoparticle Electrocatalysts for the Refinement of Theory. *Chem. Rev.* **2020**, *120*, 814–850. https://doi.org/10.1021/acs.chemrev.9b00246.

(12) Tedsree, K.; Chan, C. W. A.; Jones, S.; Cuan, Q.; Li, W. K.; Gong, X. Q.; Tsang, S. C. E. 13C NMR Guides Rational Design of Nanocatalysts via Chemisorption Evaluation in Liquid Phase. *Science* **2011**, *332*, 224–228. https://doi.org/10.1126/science.1202364.

(13) Mo, J.; Stefanov, B. I.; Lau, T. H. M.; Chen, T.; Wu, S.; Wang, Z.; Gong, X. Q.; Wilkinson, I.; Schmid, G.; Tsang, S. C. E. Superior Performance of Ag over Pt for Hydrogen Evolution Reaction in Water Electrolysis under High Overpotentials. *ACS Appl. Energy Mater.* **2019**, *2*, 1221–1228. https://doi.org/10.1021/acsaem.8b01777.

(14) Tedsree, K.; Li, T.; Jones, S.; Chan, C. W. A.; Yu, K. M. K.; Bagot, P. A. J.; Marquis, E. A.; Smith, G. D. W.; Tsang, S. C. E. Hydrogen Production from Formic Acid Decomposition at Room Temperature Using a Ag-Pd Core-Shell Nanocatalyst. *Nat. Nanotechnol.* **2011**, *6*, 302–307. https://doi.org/10.1038/nnano.2011.42.

(15) Noguera, C. Polar Oxide Surfaces. *J. Phys. Condens. Matter* **2000**, *12*, R367–R410. https://doi.org/10.1088/0953-8984/12/31/201.

(16) Ye, L.; Mahadi, A. H.; Saengruengrit, C.; Qu, J.; Xu, F.; Fairclough, S. M.; Young, N.; Ho, P. L.; Shan, J.; Nguyen, L.; Tao, F. F.; Tedsree, K.; Tsang, S. C. E. Ceria Nanocrystals Supporting Pd for Formic Acid Electrocatalytic Oxidation: Prominent Polar Surface Metal Support Interactions. *ACS Catal.* **2019**, *9*, 5171–5177. https://doi.org/10.1021/acscatal.9b00421.

(17) Kwon, S. G.; Hyeon, T. Colloidal Chemical Synthesis and Formation Kinetics of Uniformly Sized Nanocrystals of Metals, Oxides, and Chalcogenides. *Acc. Chem. Res.* **2008**, *41*, 1696–1709. https://doi.org/10.1021/ar8000537.

(18) Xia, Y.; Xiong, Y.; Lim, B.; Skrabalak, S. E. Shape-Controlled Synthesis of Metal Nanocrystals: Simple Chemistry Meets Complex Physics? *Angew. Chem. Int. Ed.* **2009**, *48*, 60–103. https://doi.org/10.1002/anie.200802248.

(19) Kitano, M.; Inoue, Y.; Yamazaki, Y.; Hayashi, F.; Kanbara, S.; Matsuishi, S.; Yokoyama, T.; Kim, S. W.; Hara, M.; Hosono, H. Ammonia Synthesis Using a Stable Electride as an Electron Donor and Reversible Hydrogen Store. *Nat. Chem.* **2012**, *4*, 934–940. https://doi.org/10.1038/nchem.1476.

(20) Li, Y.; Wu, S.; Zheng, J.; Peng, Y.-K.; Prabhakaran, D.; Taylor, R. A.; Chi, S.; Tsang, S. C. E. 2D Photocatalysts with Tuneable Supports for Enhanced Photocatalytic Water Splitting. *Mater. Today* **2020**, *41*, 34–43. https://doi.org/10.1016/j.mattod.2020.05.018.

(21) Goniakowski, J.; Finocchi, F.; Noguera, C. Polarity of Oxide Surfaces and Nanostructures. *Reports Prog. Phys.* **2008**, *71*, 1. https://doi.org/10.1088/0034-4885/71/1/016501.

(22) Wöll, C. The Chemistry and Physics of Zinc Oxide Surfaces. *Progress in Surface Science*. 2007, pp 55–120. https://doi.org/10.1016/j.progsurf.2006.12.002.

(23) Peng, Y. K.; Tsang, S. C. E. Facet-Dependent Photocatalysis of Nanosize Semiconductive Metal Oxides and Progress of Their Characterization. *Nano Today* **2018**, *18*, 15–34. https://doi.org/10.1016/j.nantod.2017.12.011.

(24) Peng, Y. K.; Fu, Y.; Zhang, L.; Teixeira, I. F.; Ye, L.; He, H.; Tsang, S. C. E. Probe-Molecule-Assisted NMR Spectroscopy: A Comparison with Photoluminescence and Electron Paramagnetic Resonance Spectroscopy as a Characterization Tool in Facet-

Specific Photocatalysis. *ChemCatChem* **2017**, *9*, 155–160. https://doi.org/10.1002/cctc.201601341.

(25) Mclaren, A.; Valdes-Solis, T.; Li, G.; Tsang, S. C. Shape and Size Effects of ZnO Nanocrystals on Photocatalytic Activity. *J. Am. Chem. Soc.* **2009**, *131*, 12540–12541. https://doi.org/10.1021/ja9052703.

(26) Liao, F.; Huang, Y.; Ge, J.; Zheng, W.; Tedsree, K.; Collier, P.; Hong, X.; Tsang, S. C. Morphology-Dependent Interactions of ZnO with Cu Nanoparticles at the Materials' Interface in Selective Hydrogenation of CO2 to CH 3OH. *Angew. Chem. Int. Ed.* **2011**, *50*, 2162–2165. https://doi.org/10.1002/anie.201007108.

(27) Ischenko, V.; Polarz, S.; Grote, D.; Stavarache, V.; Fink, K.; Driess, M. Zinc Oxide Nanoparticles with Defects. *Adv. Funct. Mater.* **2005**, *15*, 1945–1954. https://doi.org/10.1002/adfm.200500087.

(28) Li, Y.; Tsang, S. C. E. Recent Progress and Strategies for Enhancing Photocatalytic Water Splitting. *Mater. Today Sustain.* **2020**, *9*, 100032. https://doi.org/10.1016/j.mtsust.2020.100032.

(29) Liu, S.; Yu, J.; Jaroniec, M. Anatase TiO2 with Dominant High-Energy {001} Facets: Synthesis, Properties, and Applications. *Chem. Mater.* **2011**, *23*, 4085–4093. https://doi.org/10.1021/cm200597m.

(30) Liu, G.; Yang, H. G.; Pan, J.; Yang, Y. Q.; Lu, G. Q. M.; Cheng, H. M. Titanium Dioxide Crystals with Tailored Facets. *Chem. Rev.* **2014**, *114*, 9559–9612. https://doi.org/10.1021/cr400621z.

(31) Yang, H. G.; Sun, C. H.; Qiao, S. Z.; Zou, J.; Liu, G.; Smith, S. C.; Cheng, H. M.; Lu, G. Q. Anatase TiO2 Single Crystals with a Large Percentage of Reactive Facets. *Nature* **2008**, *453*, 638–641. https://doi.org/10.1038/nature06964.

(32) Peng, Y. K.; Hu, Y.; Chou, H. L.; Fu, Y.; Teixeira, I. F.; Zhang, L.; He, H.; Tsang, S. C. E. Mapping Surface-Modified Titania Nanoparticles with Implications for Activity and Facet Control. *Nat. Commun.* **2017**, *8*, 675. https://doi.org/10.1038/s41467-017-00619-z.

(33) Setvín, M.; Aschauer, U.; Scheiber, P.; Li, Y. F.; Hou, W.; Schmid, M.; Selloni, A.; Diebold, U. Reaction of O2 with Subsurface Oxygen Vacancies on TiO_2 Anatase (101). *Science* **2013**, *341*, 988–991. https://doi.org/10.1126/science.aac9659.

(34) Peng, Y.-K.; Keeling, B.; Li, Y.; Zheng, J.; Chen, T.; Chou, H. L.; Puchtler, T. J.; Taylor, R. A.; Tsang, S. C. E. Unravelling the Key Role of Surface Features behind Facet-Dependent Photocatalysis of Anatase TiO_2. *Chem. Commun.* **2019**, *55*, 4415–4418. https://doi.org/10.1039/c9cc01561b.

(35) Mahadi, A. H.; Ye, L.; Fairclough, S. M.; Qu, J.; Wu, S.; Chen, W.; Papaioannou, E. I.; Ray, B.; Pennycook, T. J.; Haigh, S. J.; Young, N. P.; Tedsree, K.; Metcalfe, I. S.; Tsang, S. C. E. Beyond Surface Redox and Oxygen Mobility at Pd-Polar Ceria (100) Interface: Underlying Principle for Strong Metal-Support Interactions in Green Catalysis. *Appl. Catal. B Environ.* **2020**, *270*, 118843. https://doi.org/10.1016/j.apcatb.2020.118843.

(36) Trovarelli, A. Structural and Oxygen Storage/Release Properties of CeO2-Based Solid Solutions. *Comments Inorg. Chem.* **1999**, *20*, 263–284. https://doi.org/10.1080/02603599908021446.

(37) Acerbi, N.; Tsang, S. C. E.; Jones, G.; Golunski, S.; Collier, P. Rationalization of Interactions in Precious Metal/Ceria Catalysts Using the d-Band Center Model. *Angew. Chem. Int. Ed.* **2013**, *52*, 7737–7741. https://doi.org/10.1002/anie.201300130.

(38) Sun, C.; Li, H.; Chen, L. Nanostructured Ceria-Based Materials: Synthesis, Properties, and Applications. *Energy Environ. Sci.* **2012**, *5*, 8475–8505. https://doi.org/10.1039/c2ee22310d.

(39) Trovarelli, A.; Llorca, J. Ceria Catalysts at Nanoscale: How Do Crystal Shapes Shape Catalysis? *ACS Catal.* **2017**, *7*, 4716–4735. https://doi.org/10.1021/acscatal.7b01246.

(40) Tan, Z.; Li, G.; Chou, H.-L.; Li, Y.; Yi, X.; Mahadi, A. H.; Zheng, A.; Edman Tsang, S. C.; Peng, Y.-K. Differentiating Surface Ce Species among CeO 2 Facets by Solid-State NMR for Catalytic Correlation. *ACS Catal.* **2020**, *10*, 4003–4011. https://doi.org/10.1021/acscatal.0c00014.

(41) Li, H. Y.; Wang, H. F.; Guo, Y. L.; Lu, G. Z.; Hu, P. Exchange between Sub-Surface and Surface Oxygen Vacancies on CeO_2(111): A New Surface Diffusion Mechanism. *Chem. Commun.* **2011**, *47*, 6105–6107. https://doi.org/10.1039/c1cc11226k.

(42) Zhao, Y.; Eley, C.; Hu, J.; Foord, J. S.; Ye, L.; He, H.; Tsang, S. C. E. Shape-Dependent Acidity and Photocatalytic Activity of Nb 2O 5 Nanocrystals with an Active TT (001) Surface. *Angew. Chem. Int. Ed.* **2012**, *51*, 3846–3849. https://doi.org/10.1002/anie.201108580.

(43) Zhou, X.; Qu, J.; Xu, F.; Hu, J.; Foord, J. S.; Zeng, Z.; Hong, X.; Edman Tsang, S. C. Shape Selective Plate-Form Ga2O3 with Strong Metal–Support Interaction to Overlying Pd for

Hydrogenation of CO_2 to CH_3OH. *Chem. Commun.* **2013**, *49*, 1747–1749. https://doi.org/10.1039/c3cc38455a.

(44) Qu, J.; Zhou, X.; Xu, F.; Qu, J.; Chi, S.; Tsang, E. Shape Effect of Pd Promoted Ga_2O_3 Nanocatalysts for Methanol Synthesis from CO2 Hydrogenation. *J. Phys. Chem. C* **2014**, *118*, 24452–24466.

(45) Airo, M. A.; Gqoba, S.; Otieno, F.; Moloto, M. J.; Moloto, N. Structural Modification and Band-Gap Crossover in Indium Selenide Nanosheets. *RSC Adv.* **2016**, *6*, 40777–40784. https://doi.org/10.1039/c6ra00262e.

(46) Liu, F.; You, L.; Seyler, K. L.; Li, X.; Yu, P.; Lin, J.; Wang, X.; Zhou, J.; Wang, H.; He, H.; Pantelides, S. T.; Zhou, W.; Sharma, P.; Xu, X.; Ajayan, P. M.; Wang, J.; Liu, Z. Room-Temperature Ferroelectricity in CuInP2S6 Ultrathin Flakes. *Nat. Commun.* **2016**, *7*, 12357. https://doi.org/10.1038/ncomms12357.

(47) Chen, Z.; Chen, Z.; Kuo, C. Y.; Tang, Y.; Dedon, L. R.; Li, Q.; Zhang, L.; Klewe, C.; Huang, Y. L.; Prasad, B.; Farhan, A.; Yang, M.; Clarkson, J. D.; Das, S.; Manipatruni, S.; Tanaka, A.; Shafer, P.; Arenholz, E.; Scholl, A.; Chu, Y. H.; Qiu, Z. Q.; Hu, Z.; Tjeng, L. H.; Ramesh, R.; Wang, L. W.; Martin, L. W. Complex Strain Evolution of Polar and Magnetic Order in Multiferroic BiFeO3 Thin Films. *Nat. Commun.* **2018**, *9*, 3764. https://doi.org/10.1038/s41467-018-06190-5.

(48) Liu, G.; Robertson, A. W.; Li, M. M. J.; Kuo, W. C. H.; Darby, M. T.; Muhieddine, M. H.; Lin, Y. C.; Suenaga, K.; Stamatakis, M.; Warner, J. H.; Tsang, S. C. E. MoS2 Monolayer Catalyst Doped with Isolated Co Atoms for the Hydrodeoxygenation Reaction. *Nat. Chem.* **2017**, *9*, 810–816. https://doi.org/10.1038/NCHEM.2740.

(49) Lau, T. H. M.; Wu, S.; Kato, R.; Wu, T. S.; Kulhavý, J.; Mo, J.; Zheng, J.; Foord, J. S.; Soo, Y. L.; Suenaga, K.; Darby, M. T.; Tsang, S. C. E. Engineering Monolayer 1T-MoS2 into a Bifunctional Electrocatalyst via Sonochemical Doping of Isolated Transition Metal Atoms. *ACS Catal.* **2019**, *9*, 7527–7534. https://doi.org/10.1021/acscatal.9b01503.

(50) Mo, J.; Wu, S.; Lau, T. H. M.; Kato, R.; Suenaga, K.; Wu, T. S.; Soo, Y. L.; Foord, J. S.; Tsang, S. C. E. Transition Metal Atom–Doped Monolayer MoS2 in a Proton-Exchange Membrane Electrolyzer. *Mater. Today Adv.* **2020**, *6*, 100020. https://doi.org/10.1016/j.mtadv.2019.100020.

(51) Lau, T. H. M.; Lu, X.; Kulhavý, J.; Wu, S.; Lu, L.; Wu, T. S.; Kato, R.; Foord, J. S.; Soo, Y. L.; Suenaga, K.; Tsang, S. C. E. Transition Metal Atom Doping of the Basal Plane of MoS_2 Monolayer Nanosheets for Electrochemical Hydrogen Evolution. *Chem. Sci.* **2018**, *9*, 4769–4776. https://doi.org/10.1039/c8sc01114a.